Full Text View

Volume 29, Issue 9 (September 1999)

Journal of Physical Oceanography
Article: pp. 2183–2190 | Abstract | PDF (154K)

The Observed Dispersion Relationship for North Pacific Rossby Wave Motions

Xiaoyun Zang and Carl Wunsch

Program in Atmospheres, Oceans, and Climate, Department of Earth, Atmospheric and Planetary Sciences, Massachusetts Institute of Technology, Cambridge, Massachusetts

(Manuscript received June 3, 1998, in final form September 8, 1998)

DOI: 10.1175/1520-0485(1999)029<2183:TODRFN>2.0.CO;2

ABSTRACT

The phase speeds of ocean surface height variability obtained by analyzing the time–longitude sections of altimetric anomalies have been widely reported as being generally faster than those of free, first baroclinic linear mode flat-bottom Rossby (planetary) waves. In contrast to previous analyses, extraction of the different signals in the time–longitude domain is performed here by array processing methods better able to separate different frequency and wavenumber bands. Although an incomplete description of oceanic variability in the North Pacific, real oceanic motions with energy levels varying from about 10% to 40% of the total in each frequency band are indistinguishable from the simplest theoretical description. At higher latitudes, as the linear waves slow, they disappear altogether. Nonequatorial latitudes display some energy with frequencies too high for consistency with linear theory; this energy produces a positive bias if a lumped average westward phase speed is computed for all the motions present.

1. Introduction

Rossby, or planetary, waves are the fundamental low-frequency modes of the ocean circulation. In a recent paper, Chelton and Schlax (1996, hereafter CS) used observations of sea surface topography from satellite altimetry to conclude that there was a systematic discrepancy between the linear theory for the zonal phase speed c_n of these waves and what they were observing in a frequency band between ½ and 2 cycles per year. Their result was immediately rationalized in several ways. Qiu et al. (1997), extending a previous study by White (1977), showed that motions that were the sum of a free wave plus a forced pattern could produce apparent zonal phase speeds near $2c_n$. Killworth et al. (1997) demonstrated that the presence of mean

zonal flows could affect phase propagation in two ways: through advection and through the modification of the mean potential vorticity gradient (the index of refraction for the waves).

The CS analysis was based upon "stacking" longitude–time diagrams (their footnote number 28). But oceanic motions are fundamentally "broadband" in character in both frequency and wavenumber terms (see, e.g., the spectral estimates of Wunsch and Stammer 1995; Stammer 1997a). A rigorous determination of phase velocity in a broadband situation requires isolating narrowband frequencies and wavenumbers so as to, among other things, clearly distinguish the phase and group velocities in longitude–time diagrams. Apart from the important question as to whether the low oceanic modes are in accord with theory, one seeks an understanding of the observed spectral distribution and its breakdown in directionally propagating components. Using wavelet transforms, Wang et al. (1998) identified two types of Rossby waves with different frequencies and wavenumbers along 25°S. Their particular method was unable to separate eastward- from westward-going motion however, and no estimates of uncertainty could be provided.

In this paper, we revisit the CS analysis in the North Pacific Ocean, but employ standard array processing methods to produce narrowband frequency–wavenumber estimates. Anticipating the conclusions below, we find some motions at all locations that are indistinguishable from the results of the most elementary theory. The remaining energy requires more complex explanation.

2. A bit of theory and preliminary observations

As in CS and in many other references, for the simplest case of linear, flat-bottom motions the dispersion relationship for Rossby waves[1] can be written

$$\sigma(k,\ l,\ n) = -\frac{\beta(y)k}{k^2 + l^2 + 1/R_n^2(x,\ y)}, \qquad \sigma > 0. \quad (1)$$

Here σ is the frequency, (k, l) is the local Cartesian wavenumber, β is the meridional gradient of the Coriolis parameter, and R_n is the Rossby radius of deformation for vertical modes $n = 0, 1, 2, \ldots$; x, y are local Cartesian zonal and meridional coordinates. We make the convention $\sigma > 0$, $k < 0$ so that westward phase speeds $c_n < 0$. (From here on, "phase speed" is taken to be only the zonal component of velocity.) The barotropic mode, $n = 0$, has a deformation radius of thousands of kilometers, while $R_1 = O(35$ km) with smaller values for correspondingly higher vertical modes. Both β and R_n are slowly varying functions of y, and these variations have practical consequences for the data analysis. Note that for any given mode at a fixed latitude, there is a maximum frequency (shortest period) given by

$$\sigma_{n-\max} = \frac{\beta R_n}{2}, \qquad n \geq 1. \quad (2)$$

To the extent that waves satisfying Eq. (1) actually exist in the ocean, they manifest themselves at the sea surface by appearing along the surface $\sigma(k, l, n)$. These waves are, in principle, separable by three-dimensional Fourier analysis. But the extent of the sea surface signature depends upon the vertical mode structure. In a study of current meter moorings, Wunsch (1997) inferred that the surface kinetic energy (surface slope) would be dominated over much of the globe by the first baroclinic mode, with higher modes tending to greater importance at low latitudes and near some boundaries. The barotropic mode, although often energetically dominant, is eclipsed at the sea surface by the intensification there of the vertical structures of the baroclinic modes. The situation for elevation, rather than slope, is less clear [but see the GCM results of Fukumori et al. (1998) showing strong barotropic dominance at high latitudes]. First-mode elevation dominance was assumed by CS, but one must anticipate contributions from all the modes.

3. Data and data processing

Here, following CS, we use TOPEX/Poseidon (T/P) altimeter data, from the period 1 January 1993 to 21 September 1997, edited and corrected as described by King et al. (1994) except for the use of a more recent tidal model. The dataset available to CS spanned about three years. Here the five years of data improves both the frequency resolution and the statistical reliability. TOPEX/Poseidon provides global sea surface height observations every 9.91 days. Data within an orbit cycle were assigned to a common time. This assignment will have a distorting effect on the result, but as will be seen, the results suggest it is not of first-order importance. The time mean was removed from each alongtrack point to obtain the time-dependent part, then a three block nonoverlapping time average was performed to filter out all motions with periods shorter than 59.5 days. The result is an array of elevation anomalies $\eta'(\Phi_i, \lambda_i, t)$, where Φ is the latitude, λ the longitude, and $t = 1\Delta t, 2\Delta t, \ldots, 58\Delta t$ is a time index, with $\Delta t = 29.7$ days. A large, and large-scale, steric component exists at the annual

period in the altimetric data (see Stammer 1997b); because dynamical effects at one year are of interest here, this contribution was not removed, and we rely upon the wavenumber rejection capability of our method to separate the $k = 0$ contributions from others.

One of the difficulties with the study of Rossby waves is that the propagation is not only anisotropic, but also inhomogeneous. In particular, because the meridional variation of $f(y)$ is not linear and R_n is a function of y (and x), the phase velocities are functions of latitude. Phase lines initially aligned with a meridian will "turn" because the phase velocity is greater at low latitudes than at high latitudes (see Schopf et al. 1981). If the ocean occupied the entire globe, the proper basis set would be the spherical harmonics. In the present situation we represent the waves as sines and cosines in narrow latitude bands in a series of boxes depicted in Fig. 1 and listed in Table 1. The latitude range is restricted to 0.2° so that the meridional changes are negligible. The longitude bands are sufficiently restricted that zonal variations in R_n are slight.

Seven boxes, chosen somewhat arbitrarily to represent low, middle, and high Pacific latitudes as well as some degree of east–west dependence, are used. Consider any box centered at latitude Φ_0. Then within the box, we can think of each position of an altimetric time series as though it were part of an array (see Fig. 2),

$$\{x_i(t)\} = \{\eta'(\phi_i, \lambda_i, t)\}, \qquad 1 \le i \le N,$$

$$1\Delta t \le t \le 58\Delta t, \qquad (3)$$

where $x_i(t)$ is the time series at pseudo-sensor i and analyze it by standard "beamforming" techniques (e.g., Capon 1969; Lacoss 1971; Båth 1974; a brief summary is given in the appendix). An alternative procedure would be direct three-dimensional least squares fitting of sines and cosines; array processing procedures are, however, efficient and convenient.

Because of the "diamond pattern" in which the satellite ground tracks cover the ocean, we can choose analysis positions Φ_i, λ_i within the boxes either with a regular or irregular spacing along and between these tracks. The zonal spacing between sensors is vanishingly small near where the descending and ascending arcs intersect. So-called data-adaptive techniques for array processing are well known, especially Capon's (1969) method. These methods are most powerful when arrays are small and irregular, and the plane-wave signal-to-noise ratio is large. In the present case, we arrange for the data coverage to be fairly uniform and large scale, and the Capon method did not produce better results than did the more robust and conventional beamforming method. An attempt to examine high wavenumbers by employing a very disparate array spacing and the Capon method will be described briefly at the end.

After filtering, each "sensor" has an altimetric time series $x_i(t)$ at intervals, $\Delta t = 29.7$ days, with duration $T = 58\Delta t$. To stabilize the cross-power estimates (see the appendix), frequency-band averaging was done over three adjacent values that thus sets the approximate frequency resolution of the analysis. Let the zonal width of the array (its aperture) be L, and let the smallest zonal spacing between any two elements be Δr (in kilometers). Beam forming produces estimates of the power density $\Phi(\sigma, k, l)$ in a band of zonal wavenumbers, $2\pi/L \lesssim k \lesssim \pi/(\Delta r)$. Each box extends sufficiently far in the zonal direction to distinguish the first-mode baroclinic wave from motions at or near $k = 0$. This k-wavenumber band is separately computed for each of the resolved frequencies. Because the meridional aperture is so small, there is almost no resolving power in the meridional direction (wavenumber l), which is therefore, indistinguishable from $l = 0$ in the results.

4. Results

a. Area 4

Consider Area 4, northwest of the Hawaiian chain. Figure 2 depicts positions for which altimetric time series were generated, thus defining the array. Figure 3a shows the so-called beam pattern of the array, which can be interpreted as the apparent wavenumber spectrum that would be centered on wavenumber (k_0, l_0) if there were a monochromatic wave of this wavenumber at a fixed frequency crossing the array. Notice that only a very narrow meridional wavenumber band is shown because of the lack of resolution in the north–south direction. Figures 3b–f show the result of the analysis at frequencies plotted as $\log_{10}[\Phi(\sigma, k, l)/\Phi_{\max}(\sigma, k, l)]$ with an asterisk denoting the position of the computed maximum. As expected, the energy density is generally much larger for negative wavenumbers (westward phase velocity) than for eastward going motions. There is a finite background energy at all wavenumbers upon which the peaks are superimposed. This background continuum, which generally has more energy than is found in the plane-wave peak, requires separate study.

Because the analysis is essentially a two-dimensional (σ, k) one and the $l = 0$ waves are the fastest ones, Fig. 4 depicts

the dispersion relations for the barotropic and first baroclinic modes in Area 4, with $l = 0$ (first baroclinic Rossby radii are from Chelton et al. 1998). The observed spectral peaks have been transferred from Fig. 3 to Fig. 4, and an uncertainty estimate is generated from the confidence limits derived by Capon and Goodman (1970) and as described in the appendix. An indication of the relative strength of the peak is provided by the circle diameter. The only observed spectral peaks are on the longwave branch (wavenumbers below the wavenumber corresponding to the maximum frequency for mode 1). With one exception, at a frequency near 0.008 cycles/day (period 123 days), the observed peaks are indistinguishable within error estimates from the conventional linear dispersion curves. For the comparatively weak motions lying at frequencies $\sigma > \sigma_{1-\max}$ the motions cannot be explained as linear baroclinic waves. The fraction of the energy lying in the observed peak varies from about 43% near 862-day period declining monotonically to about 11% at 157-day period.

The zonal group velocity vanishes at $\sigma = \sigma_{n-\max}$, and under some circumstances (e.g., Wunsch and Gill 1976) one anticipates an energy density maximum here in a form of resonance. We see no evidence for such motions.

1) PHASE SPEED

By definition, the (zonal) phase speed of a wave is $c = \sigma/k$, the slope of the dispersion curve. For those frequencies and wavenumbers in Fig. 4 lying on or near the dispersion curves, the observed and theoretical phase speeds are in accord within the uncertainty limits. At higher frequencies (or absolute wavenumbers), the observed frequencies are systematically higher than the first baroclinic dispersion curve would permit. The average slope of the empirical dispersion curve is higher than the theoretical mean slope and one thus has a positive phase speed bias. If we rule out the possibility that the waves are barotropic motions with *too low* a phase speed, then one could fairly conclude that these waves are moving faster than theory permits.

Equally appealing, however, would be their description as motions not simply consistent with linear dynamics. Many sources of such motions are known, including wind forcing, instabilities, nonlinear self-interactions, etc. On smaller scales (mesoscale), the existence of baroclinic motions not satisfying linear dispersion relations has been known for a long time (e.g., The MODE Group 1978). Thus, if all the motions lying within a finite frequency band are used to compute an apparent overall phase velocity, irrespective of the physics present, there is clearly a bias toward large values. But the separation into distinct frequency and wavenumber regions shows that much of the motion is not in conflict with the simplest linear theory.

b. Other areas

The frequency–zonal wavenumber spectra for the remaining areas analyzed here are shown in Fig. 5. In Area 1 (Fig. 5a), most peaks are located at $k = 0$. These motions have zonal scales larger than the array aperture and can be due to large-scale barotropic motions or steric forcing on large zonal scales (annual cycle heating) or both. Only two peaks are not located at $k = 0$ and they agree very well with the dispersion curve for first baroclinic Rossby waves, but carry only about 10% of the energy. Here again, a lumped apparent phase speed would be biased high.

As shown in Fig. 1, the latitudes of Areas 2 and 3 are the same, east and west respectively of the Hawaiian chain. The frequency–zonal wavenumber spectra for these areas are shown in Figs. 5b,c. As indicated in Table 1, long first baroclinic mode waves propagate faster in the western parts of the basin. This zonal change of phase speed is a result of the deepening of the thermocline in the west (Chelton et al. 1998). At the annual frequency band, Area 3 is dominated by a first baroclinic Rossby wave, whereas Area 2 is dominated by a signal indistinguishable from zonal uniformity ($k = 0$), which is presumably the steric contribution alluded to above. One explanation for this difference (e.g., Chelton and Schlax 1996) is that the Hawaiian Ridge generates a westward moving train of annual-period Rossby waves. Figures 5b and 5c show that at low frequencies the observed spectral peaks are located either very close to the baroclinic dispersion curve (around 20% of the total energy) or at the axis, $k = 0$. At frequencies higher than $\sigma_{1-\max}$, the observed spectral peaks are situated between the barotropic and first baroclinic Rossby wave dispersion curves.

As the latitude increases, the maximum frequency and the phase speed of the lowest baroclinic mode (the fastest baroclinic mode) decrease. Whatever baroclinic motion is present above $\sigma_{1-\max}$, it cannot be a linear flat-bottom mode. Even where the waves are present in linear theory, they become much more susceptible to the various effects described by Killworth et al. (1997) and others.

White (1977) inferred the existence of annual-period baroclinic Rossby waves in the tropical Pacific and suggested that they are generated by the annual-period wind forcing. Here we find that only Areas 3 and 4 show such waves significantly present. Other regions are dominated by energy indistinguishable from $k = 0$ and which may be spectral leakage from the annual period.

Within the equatorial band from 10°N to 10°S, CS (their Fig. 5) found that apparent westward phase speeds were smaller than the theoretical value. At these latitudes, one expects that higher modes should become more prominent, and this is observed in current meter records (e.g., Wunsch l997) and in data from profiling devices (e.g., Eriksen 1981). The unaccounted-for-presence of high modes is consistent with a negatively biased value for c_1. Furthermore, around the equator eastward propagating Kelvin and mixed Rossby–gravity wave modes become possible. The equatorial band is thus worthy of special attention, and it will not be further discussed here.

c. The short-wavelength limit

High-resolution methods permit one to use irregularly spaced arrays to seek waves whose wavelengths are set by the Nyquist wavelength of the shortest lateral separation. Robustness of the results is dependent upon signal-to-noise ratios and the actual array configuration. An attempt was made in Area 4 to determine the wavenumber spectrum at wavenumbers beyond those corresponding to $\sigma_{1-\max}$, the short-wavelength branch. No statistically significant peaks above the background energy could be found, and we will not discuss these results any further.

5. Discussion

We find a significant fraction of the energy present in the North Pacific Ocean is consistent with the linear Rossby wave dispersion relation Eq. (1). The remaining energy is not so consistent, and we believe that the results of CS are readily explained through the general mechanisms, if not all the details, described by Qiu et al. (1997), Killworth et al. (1997), and the wider literature on generalizations to more complex conditions of the linear theory. One has in part an interference pattern of free motions consistent with linear physics, superimposed upon forced motions of various types. In any fixed wavenumber band, there exist some motions with frequencies lying above the dispersion curve for first baroclinic modes. These motions produce lumped westward phase speeds that are generally too high for the linear theory. It is almost a semantic distinction as to whether the motion is best described as linear Rossby waves with the “wrong” frequency, or simply as oceanic motions not satisfying the dispersion relation. At most latitudes, there is *significant* energy that does appear consistent within present error estimates with the linear dispersion relationship.

The question raised by CS as to why c_n is too large now becomes instead the question of why frequencies become preferentially too high as wavenumber magnitudes increase. Presumably the answer to this question is some combination of the answer given by Killworth et al. (1997), the mode coupling of the barotropic and baroclinic modes known to occur in some regions (e.g., Wunsch 1997), and the space–time structure of the atmospheric forcing. Many reasons can be found for the existence of motions inconsistent with the first baroclinic mode of a resting flat-bottom ocean, including the presence of the barotropic mode, higher baroclinic modes, advection, topography, and forcing.

At higher latitudes, as the waves slow, and ultimately disappear at frequencies accessible with existing datasets, nonlinear effects as well as background distortions of the potential vorticity gradient (e.g., Killworth et al. 1997) can dominate the spectrum; eventually there is no evidence for linear waves at all.

The T/P dataset is now over six years in length and growing. With more data available, the analysis is being extended globally and to higher latitudes as part of a continuing effort to produce a fully quantitative estimate of ocean variability (Zang 1999, Ph.D. thesis in preparation). Eventually greater stability and higher-frequency resolution for the results will be obtained.

Acknowledgments

This study was supported in part by the National Science Foundation under Grant OCE 95-29545 and the National Aeronautics and Space Administration under Grant NAG 5-3724. We are indebted to D. Stammer and D. Chelton for comments and also for providing the baroclinic Rossby radius of deformation values.

REFERENCES

Båth, M., 1974: *Spectral Analysis in Geophysics.* Elsevier, 563 pp..

Capon, J., 1969: High resolution frequency–wavenumber spectrum analysis. *Proc. IEEE,* **57,** 1408–1418..

— , and N. R. Goodman, 1970: Probability distributions for estimators of the frequency–wavenumber spectrum. *Proc. IEEE,* **58,** 1785–1786..

Chelton, D. B., and M. G. Schlax, 1996: Global observations of oceanic Rossby waves. *Science*, **272,** 234–238..

— , R. A. de Szoeke, M. G. Schlax, K. El Naggar, and N. Siwertz, 1998: Geographical variability of the first baroclinic Rossby radius of deformation. *J. Phys. Oceanogr.*, **28,** 433–460.. Find this article online

Eriksen, C. C., 1981: Deep currents and their interpretation as equatorial waves in the western Pacific Ocean. *J. Phys. Oceanogr.*, **11,** 48–70.. Find this article online

Fukumori, I., R. Raghunath, and L.-L. Fu, 1998: Nature of global large-scale sea level variability in relation to atmospheric forcing: A modeling study. *J. Geophys. Res.*, **103,** 5493–5512..

Killworth, P. D., D. B. Chelton, and R. A. de Szoeke, 1997: The speed of observed and theoretical long extratropical planetary waves. *J. Phys. Oceanogr.*, **27,** 1946–1966.. Find this article online

King, C., D. Stammer, and C. Wunsch, 1994: The CMPO/MIT TOPEX/POSEIDON altimetric data set. Center for Global Change Science, Massachusetts Institute of Technology, Rep. 30, 33 pp. plus color plates..

Lacoss, R. T., 1971: Data adaptive spectral analysis methods. *Geophysics*, **36,** 661–675..

The MODE Group, 1978: The mid-ocean dynamics experiment. *Deep-Sea Res.*, **25,** 859–910..

Platzman, G. W., 1968: The Rossby wave. *Quart. J. Roy. Meteor. Soc.*, **94,** 225–246..

Qiu, B., W. Miao, and P. Müller, 1997: Propagation and decay of forced and free baroclinic Rossby waves in off-equatorial oceans. *J. Phys. Oceanogr.*, **27,** 2405–2417.. Find this article online

Schopf, P., D. L. T. Anderson, and R. Smith, 1981: Beta-dispersion of low frequency Rossby waves. *Dyn. Atmos. Oceans*, **5,** 187–214..

Stammer, D., 1997a: Global characteristics of ocean variability estimated from regional TOPEX/POSEIDON altimeter measurements. *J. Phys. Oceanogr.*, **27,** 1743–1769.. Find this article online

— , 1997b: Steric and wind-induced changes in TOPEX/POSEIDON large-scale sea surface topography observations. *J. Geophys. Res.*, **102,** 20 987–21 009..

Wang, L., C. Koblinsky, S. Howden, and B. Beckley, 1998: Large-scale Rossby wave in the South Pacific. *Geophys. Res. Lett.*, **25,** 179–182..

White, W. B., 1977: Annual forcing of baroclinic long waves in the tropical North Pacific. *J. Phys. Oceanogr.*, **7,** 50–61.. Find this article online

Wunsch, C., 1997: The vertical partition of oceanic horizontal kinetic energy. *J. Phys. Oceanogr.*, **27,** 1770–1793.. Find this article online

— , and R. Hendry, 1972: Array measurements of the bottom boundary layer and internal wave field on the continental slope. *Geophys. Fluid Dyn.*, **4,** 101–145..

— , and A. E. Gill, 1976: Observations of equatorially trapped waves in Pacific sea level variations. *Deep-Sea Res.*, **23,** 371–390..

— , and D. Stammer, 1995: The global frequency–wavenumber spectrum of oceanic variability estimated from TOPEX/POSEIDON altimeter measurements. *J. Geophys. Res.*, **100,** 24 895–24 910..

APPENDIX

6. Beam Forming

Beamforming techniques are a “delay and sum” form of processing in the Fourier frequency–wavenumber domain. Data, $x_i(t)$, at each position are temporally bandpass filtered, by ordinary fast Fourier transform, in a narrow band surrounding temporal frequency σ, generating the Fourier transforms $\hat{\mathbf{X}}_i(\sigma)$. All cross-power combinations $P_{ij}(\sigma) = \langle \hat{\mathbf{X}}_i(\sigma)\hat{\mathbf{X}}_j(\sigma)^* \rangle$ are formed (the asterisk denotes complex conjugation and the angle bracket average is estimated by frequency-band averaging). Denote the vector separation between positions i, j as $\Delta\mathbf{r}_{ij}$. The estimated dominant wavenumber present is obtained from the maximum over all plausible wavenumbers, $\mathbf{k}$ of

$$\Phi(\sigma, \mathbf{k}) = \Phi(\sigma, k, l) = \sum_{ij} P_{ij}(\sigma) \exp(-i\mathbf{k} \cdot \Delta\mathbf{r}_{ij}), \qquad \text{(A1)}$$

and the "beam pattern" is the field Φ over $\mathbf{k}$ evaluated in the presence of a single, monochromatic plane wave $\exp(i\mathbf{k}_0 \cdot \mathbf{r} - i\sigma t)$. Unlike methods based upon multidimensional fast Fourier methods, the spatial separations $\Delta\mathbf{r}_{ij}$ can be quite irregular. Oceanographic applications of this and related methods may be seen, for example, in Wunsch and Hendry (1972) and elsewhere.

The basic frequency resolution of this form of analysis is given by the reciprocal of the data duration, reduced by the frequency-band averaging as in an ordinary power density spectral estimate; the highest frequency estimated is given by the normal Nyquist criterion (data are uniformly spaced in time). Wavenumber resolution is similarly determined by the zonal array dimension with the spatial Nyquist determined, theoretically, by the smallest available zonal spatial separation. Because the data positions need not be uniformly spaced, the actual practical Nyquist wavenumber is dependent upon the signal-to-noise ratio.

So-called high-resolution methods, such as that of Capon (1969), are analogous to maximum entropy and related methods that rely upon strong assumptions about the nature of the signal present—in this particular case, upon the assumption that monochromatic plane waves dominate. If the assumption is true, one can obtain strong results.

Assuming the sensor outputs to be stationary Gaussian processes, Capon and Goodman (1970) showed that the random variable $\Phi(\sigma, k, l)$ is a multiple of a chi-square variable with $2M$ degrees of freedom, where M is the number of frequency bands averaged. In the present study, there are thus about six degrees of freedom. The uncertainty limits in zonal wavenumbers in Fig. 4 represent those wavenumbers where the background energy surrounding the apparent peak is larger than or equal to the lower limit of the 95% confidence interval.

Tables

Table 1. Areas chosen to analyze the frequency–wavenumber spectra. Zonal and meridional ranges, first baroclinic Rossby radius of deformation R_1 (Chelton et al. 1998), theoretical fastest phase speed of the first baroclinic long Rossby wave $C_{1-\max} = -\beta R^2_1$, and the minimum period of the first baroclinic Rossby waves in each region $T_{1-\min} = 2\pi/\sigma_{1-\max}$.

Area	Latitude (°N)	Longitude (°E)	R_1 (km)	$c_{1-\max}$ (cm s^{-1})	$T_{1-\min}$ (days)
1	11.9°–12.1°	180°–240°	91	−18.6	71
2	18.9°–19.1°	210°–250°	58	−7.4	116
3	18.9°–19.1°	150°–200°	67	−9.7	100
4	21.9°–22.1°	145°–195°	60	−7.5	114
5	27.9°–28.1°	150°–210°	47	−4.4	154
6	33.4°–33.6°	150°–190°	38	−2.7	200
7	37.9°–38.1°	150°–190°	30	−1.6	270

Click on thumbnail for full-sized image.

Figures

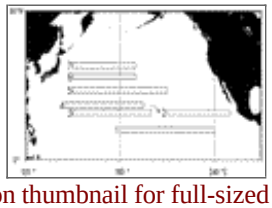

Click on thumbnail for full-sized image.

Fig. 1. Rectangles are the seven areas chosen to study the frequency wavenumber spectrum of sea surface height variability.

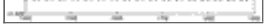

Click on thumbnail for full-sized image.

Fig. 2. Array geometry in Area 4. The position of each “sensor” is marked by a star and corresponds to a position on the TOPEX/Poseidon subsatellite track.

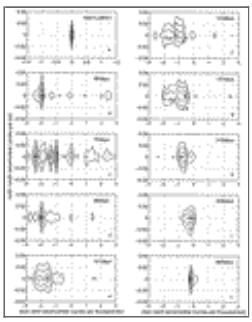

Click on thumbnail for full-sized image.

Fig. 3. The beam pattern (a) (see appendix) for the array in Fig. 2. The frequency wavenumber spectra $\Phi(\sigma, k, l)$ for Area 4 at angular frequencies (periods), $\sigma/2\pi$ (in cycles/day) ($T = 2\pi/\sigma$ in days) for (b) 0.0151 (66), (c) 0.0133 (75), (d) 0.0116 (86), (e) 0.0099 (101), (f) 0.0081 (123), (g) 0.0064 (157), (h) 0.0046 (216), (i) 0.0029 (345), and (j) 0.001 16 (862) cpd (days). The contour levels are the same in each panel and vary from 0 to −0.9 in steps of −0.3. The units of east–west wavenumber and north–south wavenumber are cycles per 1000 km and cycles per 1 km, respectively. The observed spectral peak in each frequency band is marked by a star.

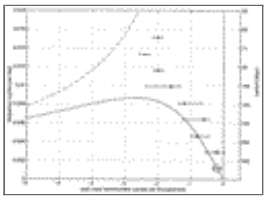

Click on thumbnail for full-sized image.

Fig. 4. Frequency–zonal wavenumber spectra of Area 4. The peak in each frequency band in Fig. 3 is indicated by a dot here. The magnitude of each peak is denoted by the size of the circle around that peak. The dash–dot and solid curves denote the barotropic and first baroclinic Rossby wave dispersion curves with $l = 0$, respectively. At the lowest frequencies, the barotropic curve is visually indistinguishable from $k = 0$. Uncertainty estimates are derived from the 95% confidence interval (Capon and Goodman 1970) for the peak values; see the appendix. The zonal wavenumber interval represents those wavenumbers where the background energy surrounding the apparent peak is larger than or equal to the lower limit of the confidence interval.

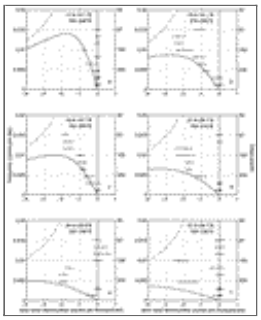

Click on thumbnail for full-sized image.

Fig. 5. Same as in Fig. 4 except (a) for Area 1, (b) Area 2, (c) Area 3, (d) Area 5, (e) Area 6, and (f) Area 7.

[1] Platzman (1968) provides a history of what have come to be called Rossby waves.

Corresponding author address: Xiaoyun Zang, Program in Atmospheres, Oceans, and Climate, Dept. of Earth, Atmospheric and Planetary Sciences, Massachusetts Institute of Technology, Cambridge, MA 02139.

E-mail: xiaoyun@pimms.mit.edu, cwunsch@pond.mit.edu